ELECTRONIC SUPPLEMENTARY INFORMATION (ESI)

ESI1. Details of the LA-SP-ICPMS simulation model

Upon LA of a biomatrix containing homogeneously distributed metal nanoparticles and dissolved metal, two distinct processes take place, associated with the nanoparticle number concentration (C_{NP}, in g^{-1}) and the dissolved metal concentration (C_{diss}, in $\mu g\ g^{-1}$), respectively. Although in both processes nanoparticles are released or generated, in general they vary in the metal content per NP and the number of NPs involved. From the dissolved metal in the matrix many thousands of NPs are generated with a very low metal content,[1] whereas from the metal NPs in the matrix significantly less NPs are released but with a 100% metal content. The former NPs are no longer detected as single NPs but associated with overlapping, superimposed NP peaks, linking them to the system response time via a washout profile.[2] The latter NPs are associated with ca. 0.5 ms events, making them detectable by "fast" ICPMS detectors as single NPs. However, under adverse conditions double, triple, etc. NPs may be detected as a single peak.

The flowchart in Figure ESI1-1 shows the procedural parameters involved in the simulation of LA-SP-ICPMS in MatLab. After generation of a pulse response profile ($FW0.01M$, in ms), this profile is randomly populated by a number of data points associated with the number of NPs entering the detector per pulse:

$$N_{NP} = 10^{-12} \cdot V \cdot D_{matrix} \cdot C_{NP} \cdot TEF \quad (1)$$

where V (in μm^3) is the volume ablated in a single laser shot, D_{matrix} is the matrix density (in $g\ cm^{-3}$), C_{NP} is the NP number concentration (in g^{-1}) and TEF is the transport efficiency factor (dimensionless). The procedure for populating the pulse response profile with NPs of size S_{NP} (in nm) is shown in Figure ESI1-2A. Following the population of the pulse response profile with same-value S_{NP} data points, the NP size variance (RSD_{NP}, in %) according to a log-normal distribution is applied in Figure ESI1-2B. After applying the NP size variance, each particle is associated with its detected MS counts via a calculation based on the following equation:

$$Ct_{NP}/N_{NP} = 10^{-21} \cdot [4/3] \cdot \pi \cdot [S_{NP}/2]^3 \cdot D_{metal} \cdot AM^{-1} \cdot AB \cdot N_A \cdot MEF \quad (2)$$

where Ct_{NP} represents the overall counts detected per pulse, Ct_{NP}/N_{NP} symbolizes the average counts detected per NP, D_{metal} is the metal NP density (in $g\ cm^{-3}$), AM is the atomic mass of the metal (in $g\ mol^{-1}$), AB is the metal isotope abundance (in $\%\ 100^{-1}$), N_A is the Avogadro constant and MEF is the measurement efficiency factor (in counts $atom^{-1}$). Figure ESI1-2C shows this conversion from size to intensity for the N_{NP}-related data points. As single N_{NP}-related data points are only generated for dwell times higher than 0.5 ms, due to the fact that NP events last ca. 0.5 ms, for dwell times $DT <$ 0.5 ms more points per NP are detected. In Figure ESI1-2D we convert the single NP-related data points to their appropriate Gaussian peaks with on average $0.5/DT$ points per peak by convolving each NP-related data point with a constant Gaussian kernel. In essence we assume that the NP peak width, or NP event, is independent of the NP size, in contrast to published data.[3,4] In ESI3 we

substantiate this assertion for LA-SP-ICPMS analysis with our 193 nm LA excimer setup and an ICPMS with a minimal dwell time of 0.1 ms; this also seems to be confirmed by other researchers.[5]

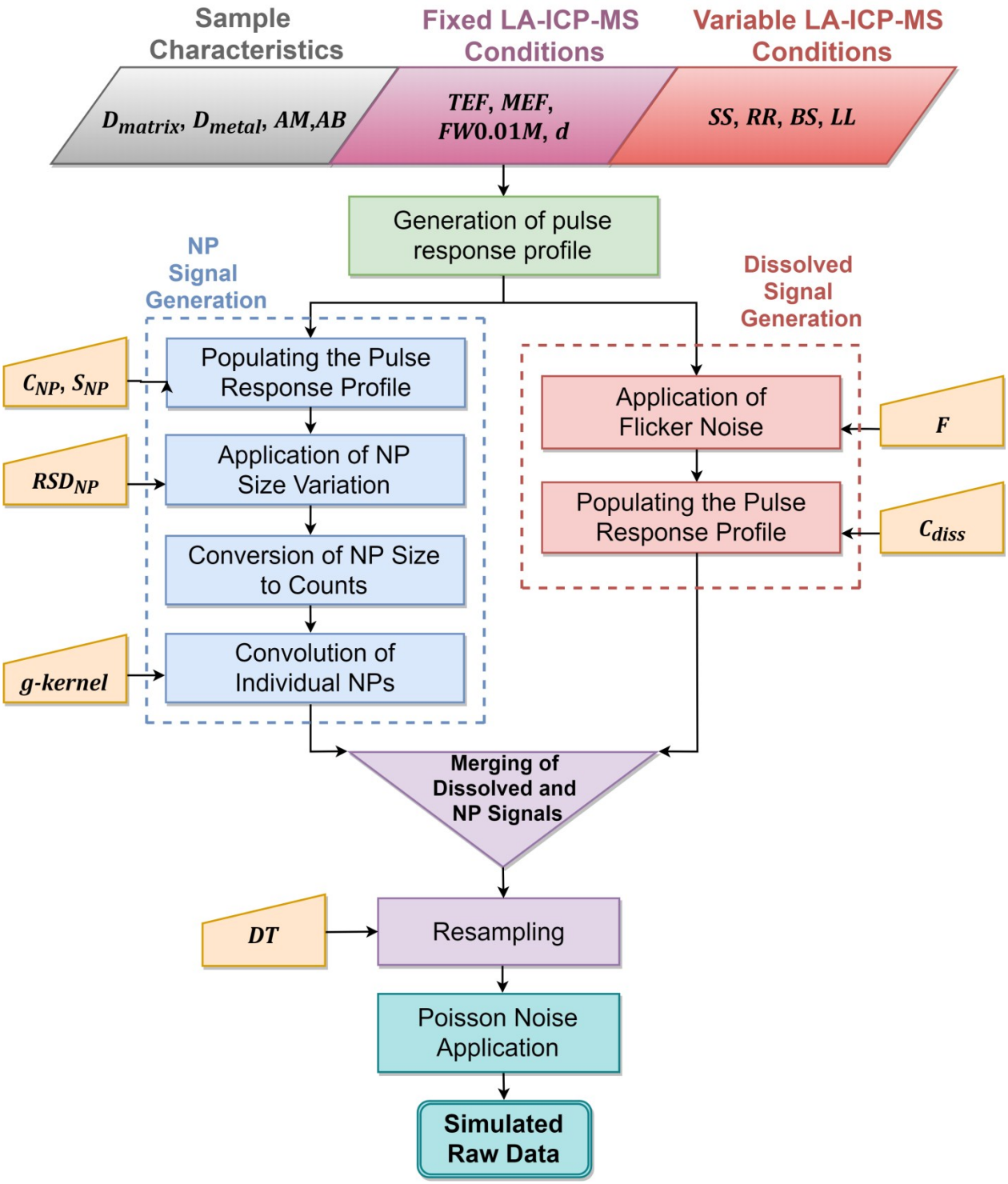

Fig. ESI1-1. Flowchart showing the procedural parameters involved in the simulation of LA-SP-ICPMS in MatLab (Table 1 in the main text gives a glossary of the terms used).

The signal for the dissolved metal in the pulse response profile is created in parallel with the NP signals. The average number of counts per pulse (Figure ESI1-3A) is calculated as follows:

$$Ct_{diss} = 10^{-18} \cdot V \cdot D_{matrix} \cdot C_{diss} \cdot TEF \cdot MEF \cdot AM^{-1} \cdot AB \cdot N_A \quad (3)$$

where Ct_{diss} (in µg g^{-1}) is the metal concentration in the biomatrix. For multiple pulses one needs to account for the variation in ablation repeatability (Figure ESI1-3B) by introducing Flicker noise (F, in %), i.e., the relative standard deviation in the pulse content over a time interval $FW0.01M$.[6] After population of the pulse profiles (Figure ESI1-3C) they need to be resampled for the dwell time DT selected (Figure SI1-3D).

After combining the data from the metal NPs and dissolved metal signals into a summated signal (see Figure 2 in the main text), Poisson noise (SD_P) is applied[6] related to the square root of the counts for a selected detection window (dwell time), which is done for each point separately.

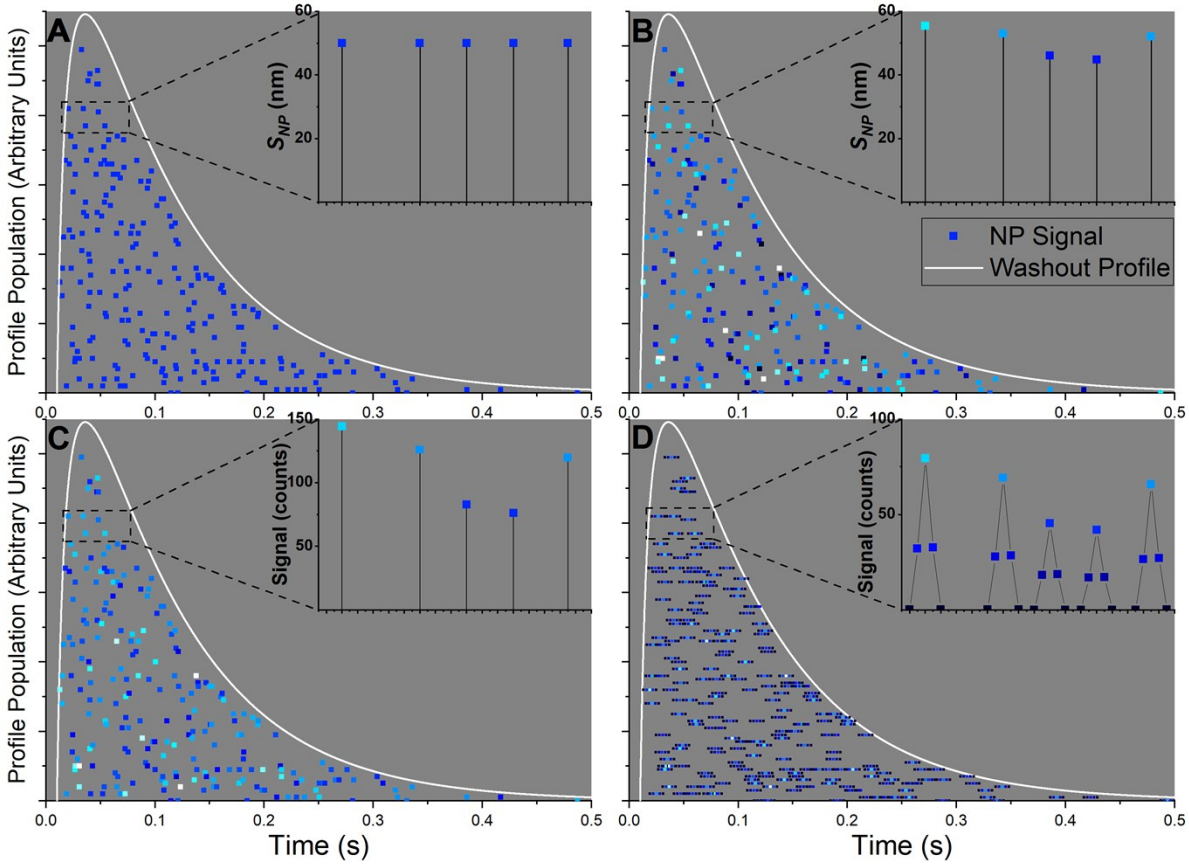

Fig. ESI1-2. Pulse response profile population steps for one pulse (A = one-size NPs distributed over the pulse profile, B = introducing the NP size variation, C = conversion of NP size into counts detected by the MS and D = convolution with a constant Gaussian kernel.

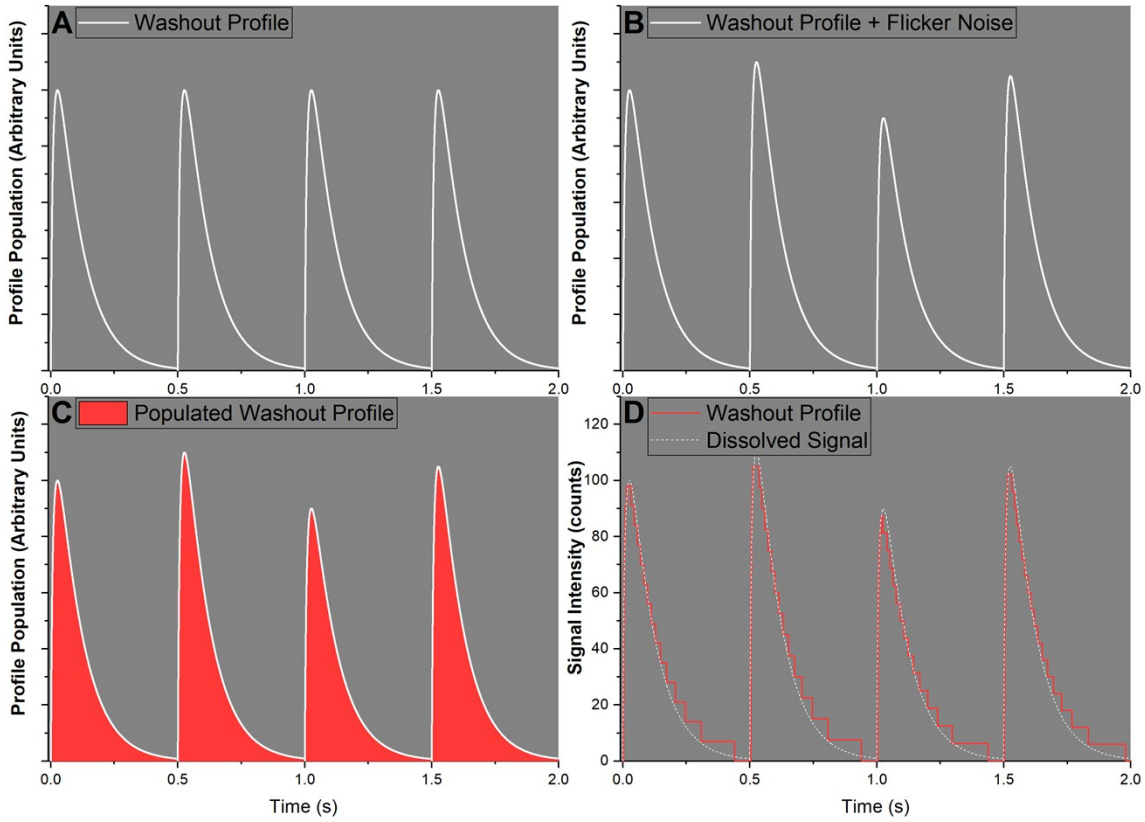

Fig. ESI1-3. Generation of the dissolved background signal response for four pulses (A = initial equal pulse profiles, B = introducing the pulse LA variability, C = population of the pulse profiles and D = resampling for a dwell time *DT*).

Finally, an optional dead time correction is applied to the resulting simulated data for each data point separately to show how larger NPs may influence the count rate negatively:

$$R_{exp} = {R_{true}}/{(1 + R_{true} \cdot \tau)} \quad (4)$$

where R_{exp} is the experimentally observed count rate (in cps), R_{true} is the true count rate (in cps) and τ is the dead time (in s). The dead time is an instrument-dependent parameter which is user-selectable in the app (enabled by default as most ICPMS instruments automatically correct for dead time cps losses).

ESI2. Retrieval of *TEF* and *MEF* values from experimental data

The *TEF* and *MEF* values can be retrieved from performing a LA-ICPMS measurement on, e.g., a gelatin standard with homogeneously distributed NPs of known size, S_{NP}, and number concentration, C_{NP}.[7] The number of nanoparticles released from the matrix per laser pulse, N_{NP},

implies that for a repetition rate *RR* the following flux of NPs entering the MS (in s^{-1}) can be calculated:

$$N_{NP} \cdot RR = 10^{-12} \cdot RR \cdot V \cdot D_{matrix} \cdot C_{NP} \quad (5)$$

with *V* (in μm^3) the volume ablated, assuming a flat-bottomed crater profile ($V=BS^2 \cdot d$ [square mask] or $V=0.25 \cdot \pi \cdot BS^2 \cdot d$ [round mask], with *d* the depth per LA shot (in μm), generally a value of ca. 0.2 μm) and D_{matrix} the matrix density (in g cm^{-3}). The transport efficiency factor, *TEF* (dimensionless), follows from counting the number of peaks per s by the MS when only single NPs are detected, $N_{NP,det}(single) \cdot RR$, and comparing them to the number of NPs entering the laser per s, N_{NP}:

$$TEF = N_{NP,det}(single)/N_{NP} \quad (6)$$

For accurate measurement of the *TEF* value it is critical that the MS detects only single NPs, thus, it is essential that a sufficiently "diluted" NP stream (flux) enters the MS by adjusting the nanoparticle number concentration, beam size, repetition rate and/or dwell time. The measurement efficiency factor, *MEF* (in counts $atom^{-1}$), can be retrieved from the same measurement based on the average counts per single nanoparticle detected ($Ct_{NP}/N_{NP,det}(single)$):

$$MEF = \left(Ct_{NP}/N_{NP,det}(single)\right)/\left(10^{-21} \cdot [4/3] \cdot \pi \cdot [S_{NP}/2]^3 \cdot D_{metal} \cdot AM^{-1} \cdot AB \cdot N_A\right) \quad (7)$$

with D_{metal} the measured metal density (in g cm^{-3}), *AB* the metal isotope abundance (in % 100^{-1}), *AM* the atomic mass of the metal isotope analyzed (in g mol^{-1}) and N_A the Avogadro constant.

ESI3. Justification for the use of a constant Gaussian kernel, independent of NP size, to construct NP peak profiles (for limited-time resolution ICPMS instruments)

In the final step of the NP signal simulation (Figure ESI1-2D), data points are convolved with a constant Gaussian kernel. In essence we assume that the NP peak width, or NP event, is independent of the NP size. This independence would show from a linear relationship between peak area *PA* (in integrated counts) vs. peak height *PH* (in counts) for differently sized NPs, based on the following Gaussian peak shape function:

$$PH = PA/\{FWHM \cdot \sqrt{\pi/(4 \cdot ln(2))}\} \quad (8)$$

When *PA* and *PH* are linearly correlated, i.e., PA/PH is a constant, the full width at half maximum, *FWHM*, is a constant as well, showing that the NP peak width is independent of the NP size. This is indeed true for our LA-SP-ICPMS setup with a limited-time resolution ICPMS (dwell time, 0.1 ms), upon measurement of NPs in the size range of ca. 20 to >100 nm, as evidenced from Figure ESI3-1. However, published data[3,4] performed with high-time resolution ICPMS instruments show that the SP-ICPMS signal duration is dependent on the NP size, changing roughly by 50% in the size range from 20 to 100 nm for gold NPs.

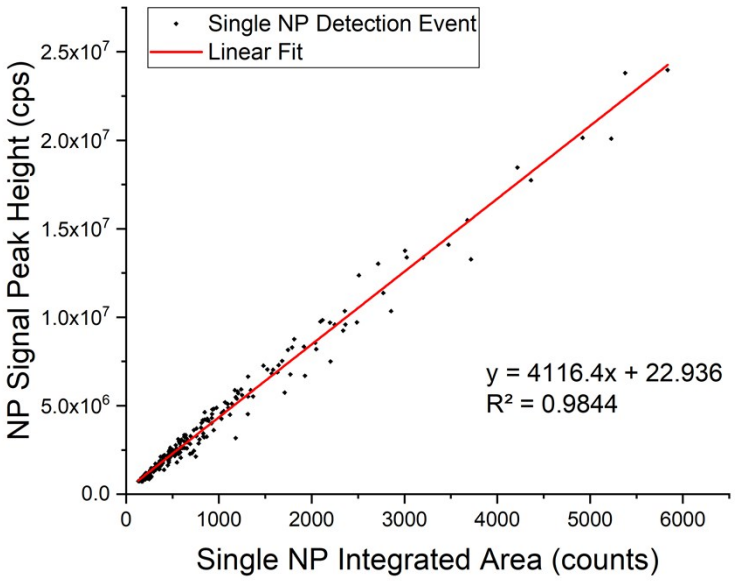

Fig. ESI3-1. Plot of NP height vs. NP area for particles in the size range of ca. 20 to >100 nm.

ESI4. Detectability as a function of the NP size for a high dissolved metal background and variable beam size

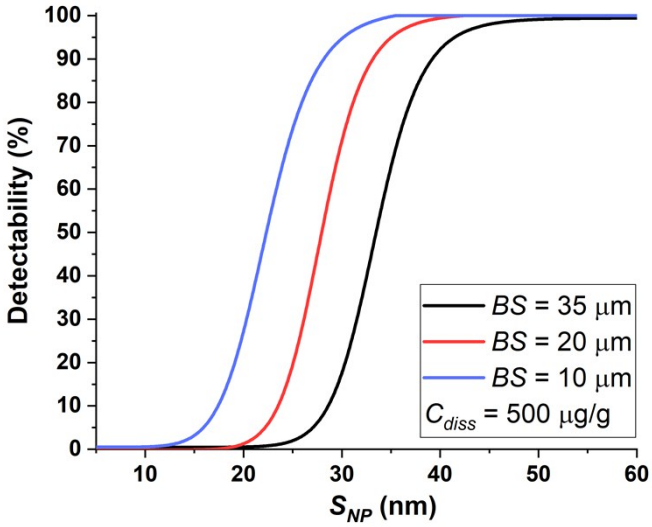

Fig. ESI4-1. Simulated detectability *DB* as a function of the NP size, S_{NP}, in the presence of a dissolved metal concentration, C_{diss}, of 500 μg g^{-1} at three beam sizes, *BS*; for other parameters see the legend of Figure 4 (main text).

REFERENCES

1 H. Nováková, M. Holá, M. Vojtíšek-Lom, J. Ondráček and V. Kanický, *Spectrochim. Acta - Part B At. Spectrosc.*, 2016, **125**, 52–60.

2 J. T. van Elteren, V. S. Šelih and M. Šala, *J. Anal. At. Spectrom.*, 2019, 1919–1931.

3 J. Fuchs, M. Aghaei, T. D. Schachel, M. Sperling, A. Bogaerts and U. Karst, *Anal. Chem.*, 2018, **90**, 10271–10278.

4 I. Strenge and C. Engelhard, *J. Anal. At. Spectrom.*, 2020, **35**, 84–99.

5 E. Bolea-Fernandez, D. Leite, A. Rua-Ibarz, T. Liu, G. Woods, M. Aramendia, M. Resano and F. Vanhaecke, *Anal. Chim. Acta*, 2019, **1077**, 95–106.

6 J. T. van Elteren, M. Šala and V. S. Šelih, *Anal. Chem.*, 2018, **90**, 5916–5922.

7 D. Metarapi, M. Šala, K. Vogel-Mikuš, V. S. Šelih and J. T. van Elteren, *Anal. Chem.*, 2019, **91**, 6200–6205.